## Electronic supplementary information

# A hybrid Si@$FeSi_y/SiO_x$ anode structure for high performance lithium-ion batteries via ammonia-assisted one-pot synthesis †

Mingxia Gao,[a] Dingsheng Wang,[a,b] Xuqing Zhang,[a] Hongge Pan,*[a] Yongfeng Liu,[a] Chu Liang,[a] Congxiao Shang,[c] Zhengxiao Guo[d]

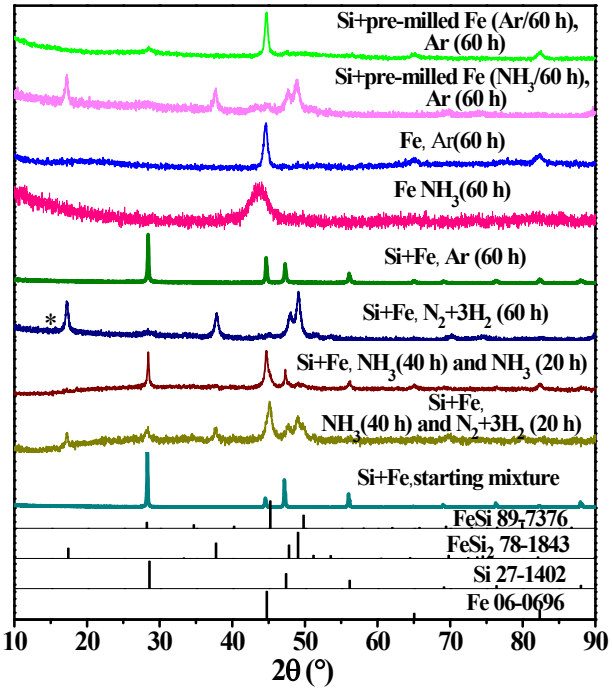


**Fig. S1** XRD patterns of the mixture of Si and Fe powders in a weight ratio of 2: 1 milled for 60 h in different atmospheres as well as the starting Si and Fe mixture; the patterns of the Fe powder milled in $NH_3$ and Ar, respectively, and further milled with Si in Ar atmosphere for 60 h. The sample with "*" (the one milled in $N_2$+3$H_2$) was rinsing in HCl solution with residual Fe removed.

**Table S1** Crystallite size and FWHM of Si ((111) facet) of the composites with different ball-milling periods as well as pristine Si

| BM periods (h) | Pristine Si | 20 | 40 | 60 | 80 | 100 |
|---|---|---|---|---|---|---|
| Crystallite size (nm) | 51 | 37 | 31 | 15 | 12 | 11 |

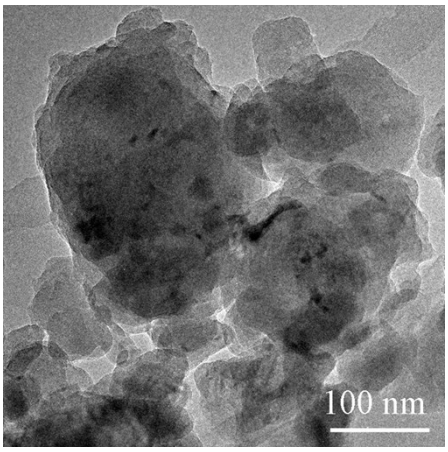


**Fig. S2** A representative TEM image of the composites, from the one of 40 h of ball-milling.

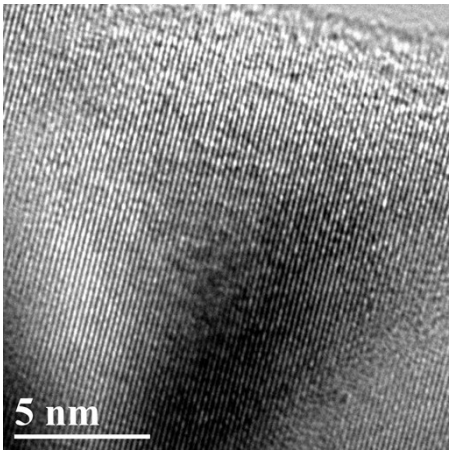


**Fig. S3** HRTEM image of the pristine Si.

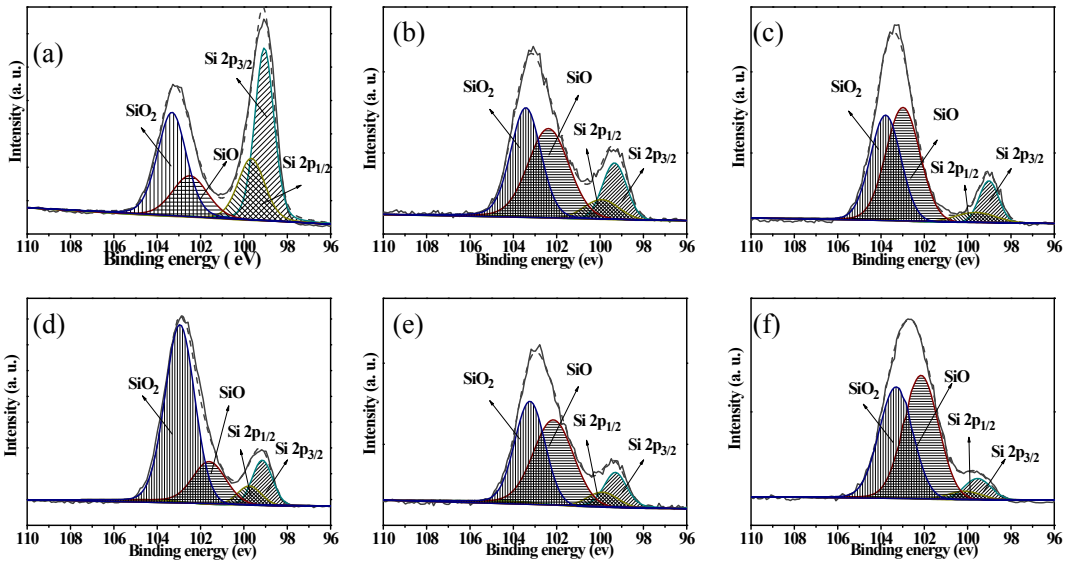


**Fig. S4** XPS spectra of the pristine Si (a) and the composites milled for 20 h (b), 40 h (c), 60 h (d), 80 h (e) and 100 h (f).

**Table S2** XPS data of the Si 2p of the pristine Si and the composites, and the molar fraction of the corresponding $Si^0$, $Si^{2+}$ and $Si^{4+}$ in the detected layers.

| Samples | Phases | | Assignment energy / eV | Molar fraction / mol% |
|---|---|---|---|---|
| Pristine Si | Si $_{2p}$ | $Si_{3/2}$ | 99.0 | 60 |
| | | $Si_{1/2}$ | 99.6 | |
| | $SiO_x$ | $Si^{2+}$ | 102.4 | 16 |
| | $x$=1.7 | $Si^{4+}$ | 103.2 | 34 |
| 20 h | Si | $Si_{3/2}$ | 99.3 | 22 |
| | | $Si_{1/2}$ | 99.9 | |
| | $SiO_x$ | $Si^{2+}$ | 102.4 | 40 |
| | $x$=1.5 | $Si^{4+}$ | 103.4 | 38 |
| 40 h | Si | $Si_{3/2}$ | 99.0 | 15 |
| | | $Si_{1/2}$ | 99.6 | |
| | $SiO_x$ | $Si^{2+}$ | 103.0 | 46 |
| | $x$=1.5 | $Si^{4+}$ | 103.8 | 39 |
| 60 h | Si | $Si_{3/2}$ | 99.1 | 21 |
| | | $Si_{1/2}$ | 99.7 | |
| | $SiO_x$ | $Si^{2+}$ | 102.1 | 41 |
| | $x$=1.5 | $Si^{4+}$ | 103.3 | 38 |
| 80 h | Si | $Si_{3/2}$ | 99.3 | 18 |
| | | $Si_{1/2}$ | 99.9 | |
| | $SiO_x$ | $Si^{2+}$ | 102.1 | 43 |
| | $x$=1.5 | $Si^{4+}$ | 103.2 | 39 |
| 100 h | Si | $Si_{3/2}$ | 99.5 | 10 |
| | | $Si_{1/2}$ | 100.1 | |
| | $SiO_x$ | $Si^{2+}$ | 102.1 | 48 |
| | $x$=1.5 | $Si^{4+}$ | 103.2 | 42 |

**Table S3** Composition of the composites detected by EDS/SEM and the values rectified by O content detected by oxygen analyzer (wt.%)

| BM periods (h) | $O_{(EDS)}$ | $Si_{(EDS)}$ | $Fe_{(EDS)}$ | $O_{(LECO)}$ | $Si_{(LECO+EDS)}$ | $Fe_{(LECO+EDS)}$ |
|---|---|---|---|---|---|---|
| 20 h | 19.4 | 77.3 | 3.3 | 19.0 | 77.7 | 3.3 |
| 40 h | 31.0 | 65.9 | 3.2 | 26.7 | 69.9 | 3.4 |
| 60 h | 5.20 | 75.2 | 19.6 | 6.2 | 74.4 | 19.4 |
| 80 h | 10.2 | 69.7 | 20.2 | 7.3 | 71.9 | 20.8 |
| 100 h | 10.5 | 68.9 | 20.6 | 8.5 | 70.4 | 21.1 |

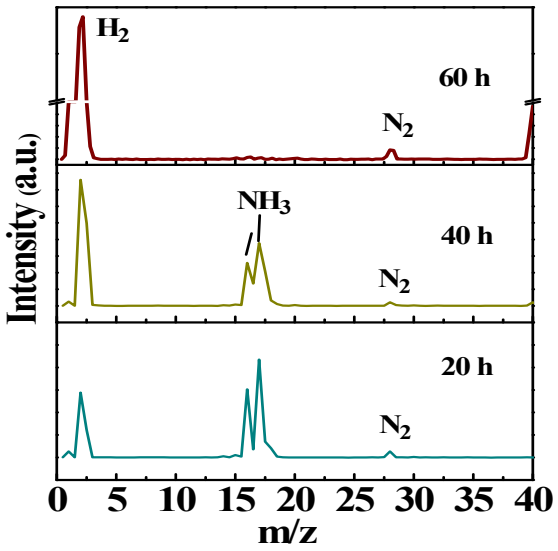


**Fig. S5** Mass spectra of the milling atmosphere after different periods of milling.

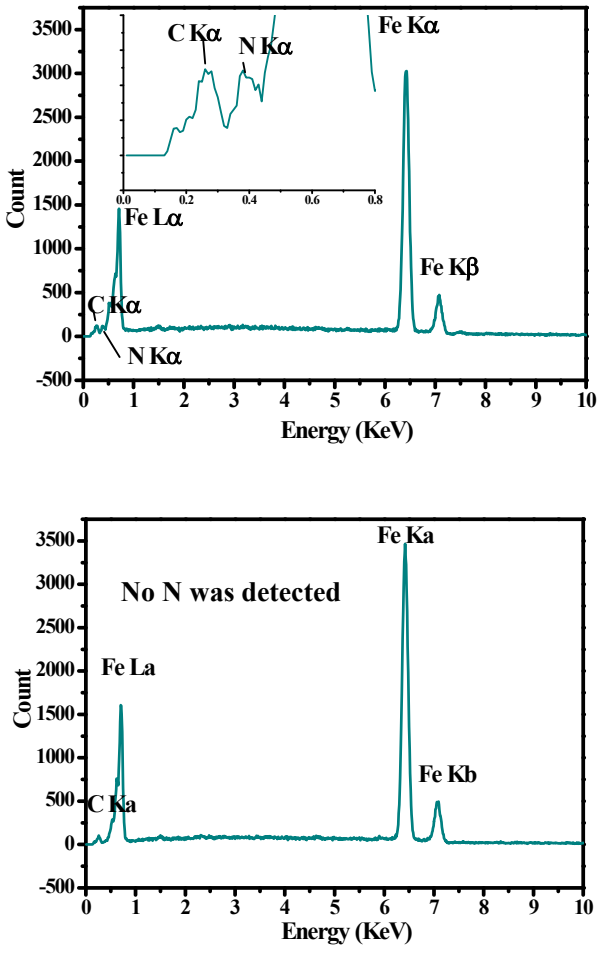


**Fig. S6** EDS patterns of the Fe powder milled in $NH_3$ (a) and in Ar (b) for 60 h.

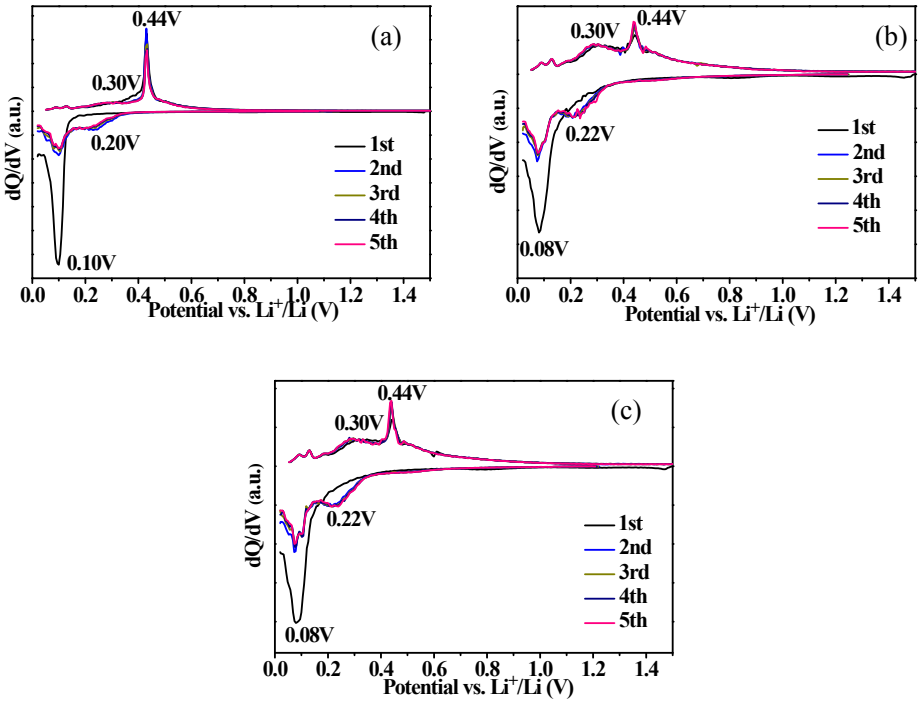


**Fig. S7** Differential capacity plots of the composites milled for 20 h (a), 80 h (b) and 100 h (c).

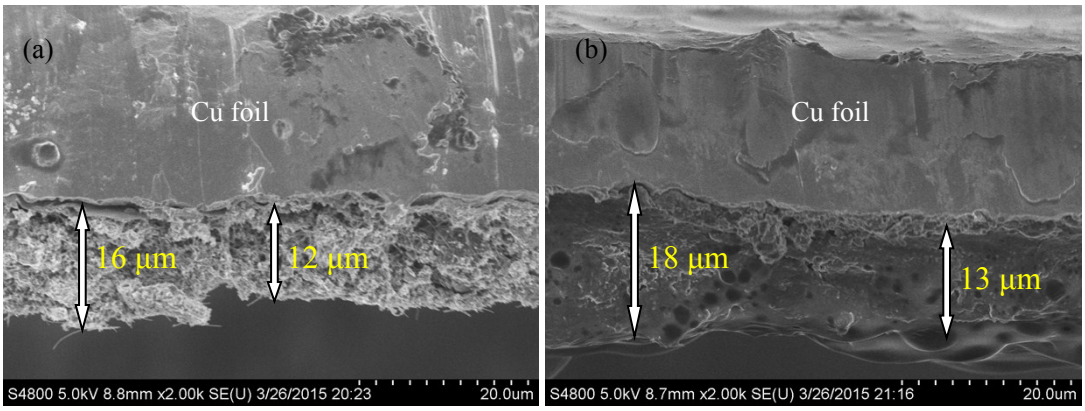


**Fig. S8** SEM images of the cross sections of the electrode of the 60 h-milled Si@$FeSi_y$/$SiO_x$ hybrid structure before (a) and after (b) initial lititaion.

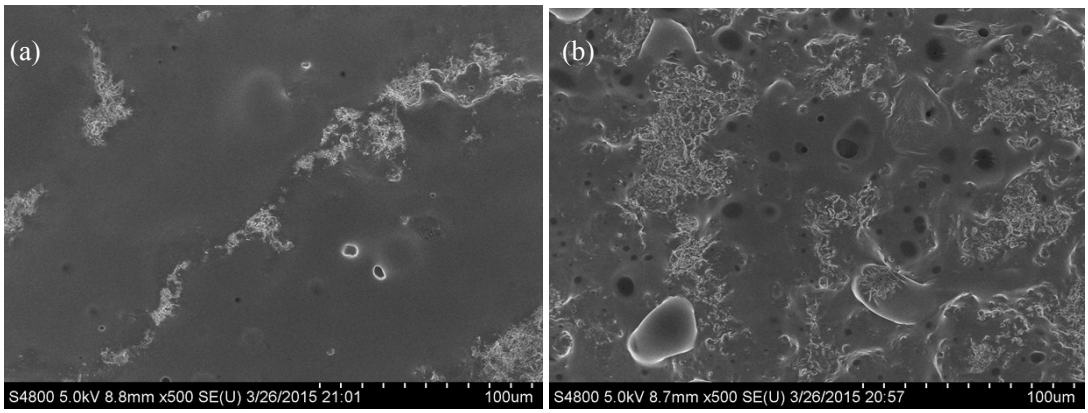


**Fig. S9** SEM images of the electrode of surface of the 60 h-milled Si@$FeSi_y/SiO_x$ hybrid structure (a) and the pristine Si (b) and after initial lititaion.